JOURNAL OF MATERIALS SCIENCE **35** (2000) 2581–2587

XPS characterisations of passive films formed on martensitic stainless steel: qualitative and quantitative investigations

M. VAYER, I. REYNAUD, R. ERRE
Centre de Recherche sur la Matière Divisée, CNRS-Université d'Orléans
1B, rue de la Férollerie, F45071 Orleans Cedex 2, France
E-mail: marylene.vayer@univ-orleans.fr

HNO_3 passivation treatments on martensitic stainless steels used for surgical instrumentation were studied. The pitting corrosion resistance was determined by electropotentiodynamic experiments. The composition and the thickness of the passive films were investigated by XPS. The pitting corrosion potential was more noble for HNO_3-passivated sample than for air-passivated sample. The different methods proposed in the literature to estimate the thickness of passive layers were used and compared. Passive films obtained by HNO_3-passivation were thinner (3 nm) than air-passivated films (4–5 nm). The composition of these passive films also differs. HNO_3-passivated films were enriched in oxidised chromium which represent half of the metallic elements in the passive layer.

1. Introduction

X20Cr13, X30Cr13, X40Cr14 martensitic stainless steels are widely used in hospitals for surgical instruments, for which corrosion resistance and mechanical properties such as hardness and cutting power are necessary. However, these instruments often rapidly corrode and so are often replaced. The corrosion resistance of these instruments depends on the origin of the martensitic stainless steel, on their surface structure (polishing state) and on the nature of the solutions in contact [1]. It can be enhanced with a passivation treatment.

The corrosion process, the influence of passivation treatments have been studied by numerous researchers [2–8] but rarely with martensitic stainless steels [2]. The pitting corrosion has been shown to be strongly affected by HNO_3 treatment. On stainless steel types 304 and 316 [9] and 430 [7], the pitting corrosion potential correlated with the amount of chromium in the surface film formed by HNO_3 treatments. Besides, Hong and Nagumo [10] have proposed that immersion in HNO_3 solution results in removal of sulphide inclusions, thus elimination of the most susceptible sites for pitting corrosion. The compositions of passive films have been studied by XPS and AES [2–5]. The corrosion resistance is closely related to chromium enrichment of the surface layer, the passivation inducing probably the formation of chromium oxy-hydroxide [6].

In previous paper [11] we demonstrated that chromium carbide inclusions are present on the surface of martensitic stainless steel and pitting corrosion yields elimination of these inclusions. No other type of inclusions has been identified.

In this paper, we focussed on composition and thickness of passive layers of martensitic stainless steels. We compared passive layer formed by a HNO_3-passivation treatment with the air-formed passive layer.

2. Experimental

2.1. Sample preparation

The examined materials were martensitic stainless steel used for surgical instrumentation. Three different alloys were used: X20Cr13, X30Cr13, X40Cr14. The chemical compositions are reported in Table I. Samples were disks of 14 mm in diameter and 5 mm in thickness. They were mechanically wet ground polished with successive 320, 500, 1200 grit silicon carbide papers and smoothed with a diamond paste (1 μm) to get a mirror finish. They were degreased with acetone and ultrasonically cleaned in ethanol.

2.2. Passivation process

The samples were HNO_3-passivated at room temperature in two steps: (a) immersion in a 50% nitric acid bath for 10 minutes, (b) rinsing with deionised water.

All the samples were examined after 24 hours of rest.

2.3. Electrochemical set up

The potentiodynamic scanning experiments were conducted with a Radiometer unit equipped with PGP201 potentiostat interfaced to a computer and a electrochemical cell with three electrodes: the working electrode was the steel sample, the counter electrode was

TABLE I Weight-% (upper lines) and atomic-% (lower lines) of the elements contained in the studied materials

	Fe	Cr	C	Si	Mn	P	S	Ni
X20Cr13	85.8	13.0	0.18	0.38	0.41	0.019	0.019	0.18
	84.1	13.7	0.82	0.74	0.41	0.030	0.010	0.17
X30Cr13	84.8	13.7	0.31	0.58	0.40	0.020	0.012	0.17
	83.1	14.4	1.41	1.13	0.40	0.035	0.006	0.16
X40Cr14	84.4	13.8	0.48	0.74	0.38	0.020	0.009	0.17
	81.7	14.3	1.94	1.43	0.37	0.035	0.015	0.16

a disk of platinum and the reference electrode was a saturated calomel electrode connected to the measured cell by a salt bridge KNO_3 and a Haber-Luggin capillary at a distance of ca 0.5 mm from the steel sample. The electrolyte used was a Hexanios solution (Anios Laboratory) at pH = 7.3 used as decontaminant of surgical instruments in hospital surrounding. This solution contained 43 ppm Cl^-.

2.4. Electrochemical measurement

The sample was first allowed sufficient time (c.a. 60 minutes) at the corrosion potential to reach an equilibrium rest potential. Then the potential scan began in anodic direction at a rate of 8 mV/min. The pitting potential (E_{pit}) was defined as the potential where the current density overstepped 100 $\mu A{\cdot}cm^2$ [10, 12]. The potential was reversed when the current density reached 1 mA. During the experiment, the temperature was kept constant at 20°C with a thermostat bath. For each condition, the experiments were repeated 20 times as the results are reproducible within 10%.

2.5. XPS analysis

XPS (X-ray Photoelectron Spectroscopy) measurements were performed on a VG ESCALAB MKII equipped with a multidetection analyser controlled by VG eclipse software, a 200 W Al K_α source and a VG EXO 5 ion gun. The basic vacuum was 10^{-7} Pa. The reference energy was the Au $4f_{7/2}$ at 84.0 eV. The structure and compositions of the passive films were determined using the depth profiling technique: The sample was periodically sputtered by argon ions (5 keV, $p\mathrm{Ar} = 6 \times 10^{-8}$ mbar, 2 $\mu A/cm^2$) and XPS spectra was recorded after each etching treatment.

The sputter rate was determined by the sputtering yield, the primary-ion current density and by the surface composition [13, 14] and the estimated value was identical within the experimental incertitude to the value determined by NRA (nuclear microanalysis). We estimated a sputter rate of 0.005 nm/s ± 0.001 nm/s.

XPS data analysis was performed with VG eclipse software and using elemental area sensitivity factors S_{ij} from the VG data base. The spectra were fitted, after background subtraction using the Shirley method, with Gaussian-Lorentzian functions. The deconvolution of a composite peak gives $I_{ij}(t)$, the measured intensity for element i in state j at time t. This can be related to the measured number $N_{ij}(t)$ of atoms per unit volume of the element i in state j at time t by the relation:

$$N_{ij}(t) = \frac{I_{ij}(t)}{S_{ij}} \tag{1}$$

The measured concentration $C^{\mathrm{M}}[i, j](t)$ of element i in state j at time t is related to $N_{ij}(t)$ by:

$$C^{\mathrm{M}}[i, j](t) = \frac{N_{ij}(t)}{\sum_{ij} N_{ij}(t)} \tag{2}$$

Such measurements, however, involve electrons which come from the material to a depth characterised by the mean escape depth $\lambda_{i,j}$ and represent an integral over this depth. The true concentration $C^{\mathrm{T}}[i, j](t)$ can be obtained by means of a simple correction to (2) [5]. This leads to

$$C^{\mathrm{T}}[i, j](t) = C^{\mathrm{M}}[i, j](t) - \frac{\lambda_{ij}}{V} * \frac{\partial C^{\mathrm{M}}[i, j](t)}{\partial t} \tag{3}$$

The mean escape depth λ were evaluated after Seah and Dench formula [15]. The values for Fe 2p, Cr 2p are estimated through an oxide layer to 1.9 and 2.1 nm.

3. Results and discussion

The pitting potential are presented in Table II. X20Cr13, X30Cr13 and X40Cr14 air-passivated material samples presented similar values of E_{pit}. Thus, there was no influence of the amount of carbon. E_{pit} were enhanced when the samples were HNO_3 passivated as often reported [6].

For each sample a XPS survey spectrum was first recorded. Only carbon, oxygen, iron, and chromium were shown on the surface. Then high resolution spectra were recorded and we identified different chemical states of these elements by means of binding energies. These values listed in Table III were in agreement with the literature [4, 16–22].

Figs 1 and 2 show respectively evolution of Cr 2p and Fe 2p spectra of X30Cr13 air-passivated and HNO_3-passivated samples during the sputtering. The spectra showed the same evolution for X20Cr13 and X40Cr14 stainless steel samples. Cr $2p_{3/2}$ core level had two contributions, a metallic one and a oxidised one. Fe $2p_{3/2}$ core level had three contributions Fe metal, Fe^{2+} oxide and Fe^{3+} oxide in increasing binding energies. The two metallic contributions were enhanced and the oxide contributions decreased with the sputtering time. Fe^{3+}

TABLE II Evolution of the pitting potential (E_{pit}) with the passivation treatment

Material	Passivation treatment	E_{pit} (mV)
X20Cr13	None	450–650
	HNO_3	950–1150
X30Cr13	None	470–670
	HNO_3	1000–1100
X40Cr14	None	500–700
	HNO_3	930–1030

TABLE III Binding energy (eV) of the chemical states of elements identified by XPS

Element	Chemical state	Binding energy (eV)
Fe $2p_{3/2}$	Fe metal	707.1 This study 706.8 [4, 16, 17]
	Fe^{2+}	709.2 This study 709.0 [17], 709.3 [16], 709.5 [4]
	Fe^{3+}	711.1 This study 711.0 [16, 17], 710.3 [4]
Cr $2p_{3/2}$	Cr metal	574.5 This study 574.1 [16], 574.2 [4], 574.8 [17]
	Cr^{3+}	576.4 This study 576.3 [16], 576.7 [4], 576.8 [17]
O1s	O^{2-}	530.3 This study 529.9 [16], 530.3 [4, 18]
	OH^-	531.5 This study 531.4 [16], 531.6 [4], 531.8 [18]
C1s	Contamination	284.6 This study 284.6 [20], 285.0 [17, 19],
	Carbide	282.8 This study 282.4 [22], 283.2 [21], 283.4 [19]

contribution was only visible at the beginning of the sputtering.

Carbon C 1s had two contributions: a contamination peak at 285.0 eV and a carbide contribution appearing at 283 eV [11]. For all unsputtered samples, C1s was one of the most intense peak. After 100 s sputtering the contamination contribution was decreased and the C1s signal was stabilised. Thus, the contamination layer was eliminated and the passive layer started, the carbon contribution was mainly the carbide present in the matrix. We evaluated the contamination layer thickness to be 0.3 nm. All the signals grew up after the elimination of the contamination layer. Oxygen O 1s had hydroxide and oxide contributions. The hydroxide contribution disappeared rapidly by sputtering (after less than 100 s). The comparison between air-passivated and HNO_3-passivated samples indicated that the air-formed passive layer contained less hydroxide than the HNO_3-passivated layer. This observation was in accordance with observations on other types of steel [4].

Fig. 3 and Fig. 4 show the C^M measured atomic concentrations of metallic Cr, oxidized Cr, metallic Fe, oxidized Fe, C and O for air-passivated and HNO_3-passivated samples of X20Cr13 during depth profiling. These profiles were identical for X30Cr13 and X40Cr14 stainless steel samples. Figs 3 and 4 highlighted the passive layer complexity.

In order to characterise passive layers, we first considered some ratio of XPS signals. $C^M[Cr2p_{3/2}]/C^M[Fe2p_{3/2}]$ evolution (Fig. 5) during XPS depth profiling was typical of the passivation treatment independently of examined stainless steel. This ration was 0.2 in the sample matrix. In passive layer,

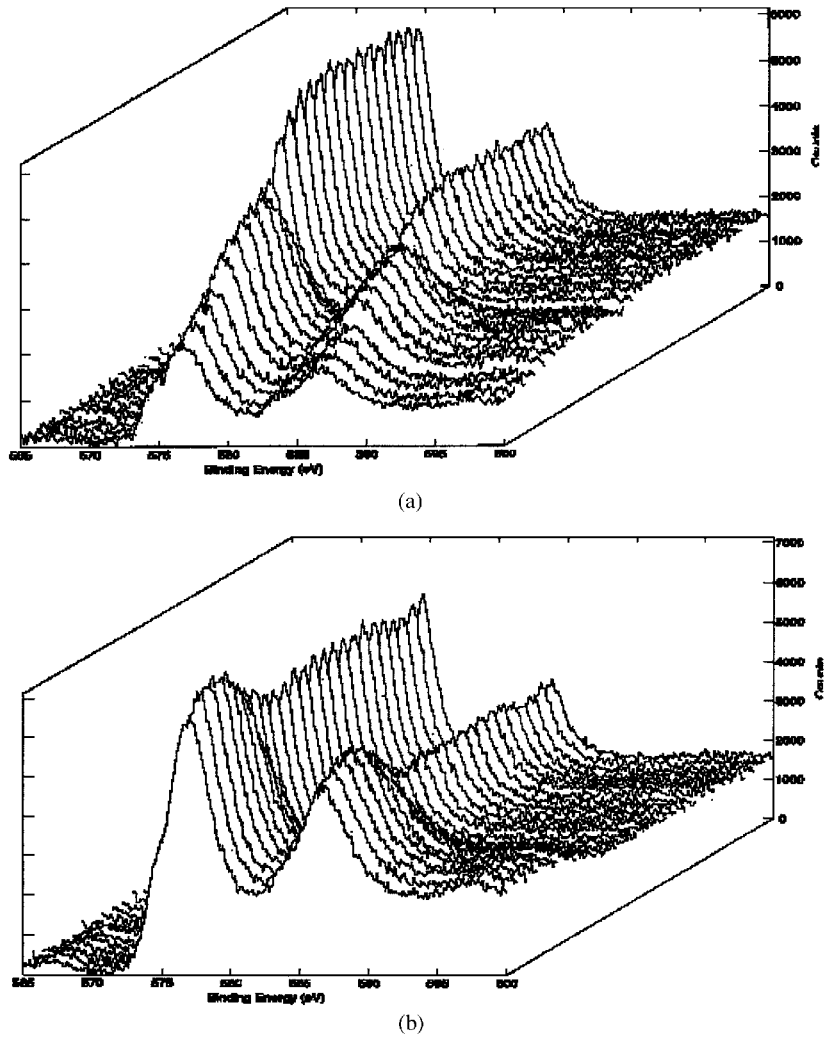

Figure 1 Evolution of the Cr 2p core level spectra of X30Cr13 stainless steel during depth profiling (a) air-passivated sample (b) HNO_3-passivated sample.

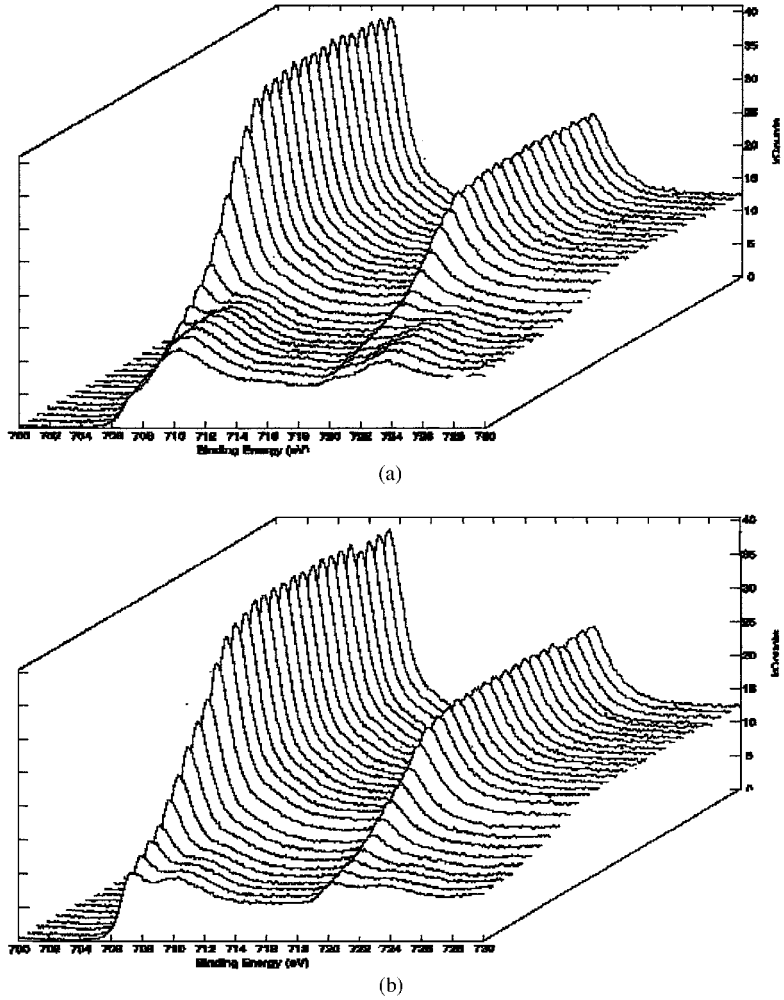

Figure 2 Evolution of the Fe 2p core level spectra of X30Cr13 stainless steel during depth profiling (a) air-passivated sample (b) HNO_3-passivated sample.

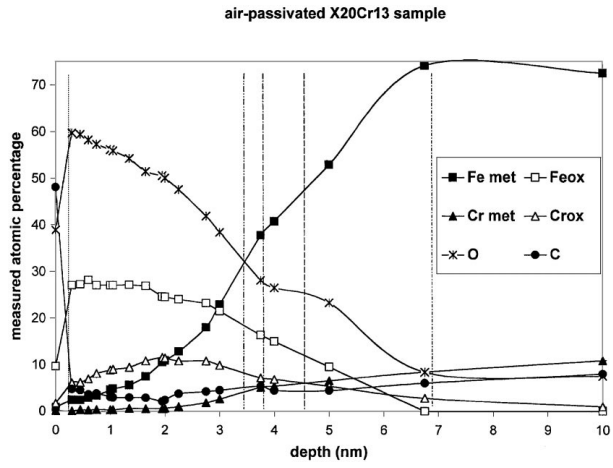

Figure 3 XPS depth profile of a air-passivated X20Cr13 stainless steel sample: the measured atomic concentrations (C^M) were reported as a function of the depth. Limits of contamination layer ……, limits of passive layer determined by $C^M[O1s] = 0.5 * C^M[O1s, ini]$ –.–.-, $C^M[Cr2p_{3/2}, oxide] = C^M[Cr2p_{3/2}, metal]$ ------, $C^M[O1s] = C^M[Fe2p_{3/2}, metal]$ –·–·–·–, the attenuation of $C^M[Fe2p_{3/2}, metal]$ ·-·-·-·-·-.

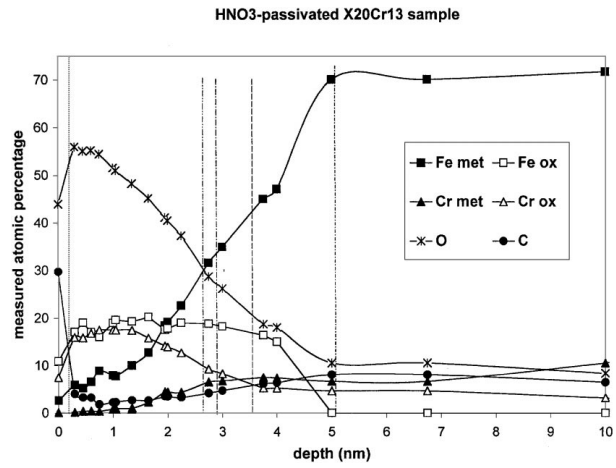

Figure 4 XPS depth profile of a HNO_3-passivated X20Cr13 stainless steel sample: the measured atomic concentrations (C^M) were reported as a function of the depth. Limits of contamination layer ……, limits of passive layer determined by $C^M[O1s] = 0.5 * C^M[O1s, ini]$ –.–.-, $C^M[Cr2p_{3/2}, oxide] = C^M[Cr2p_{3/2}, metal]$ ------, $C^M[O1s] = C^M[Fe2p_{3/2}, metal]$ –·–·–·–, the attenuation of $C^M[Fe2p_{3/2}, metal]$ ·-·-·-·-·-.

this ratio was always greater. For a HNO_3-passivated sample, $C^M[Cr2p_{3/2}]/C^M[Fe2p_{3/2}]$ decreased monotonically in the passive layer from 0.7 to 0.2. For a air-passivated sample, $C^M[Cr2p_{3/2}]/C^M[Fe2p_{3/2}]$ started from 0.2 grew to 0.35 and then went down to 0.2. There is always a Cr enrichment of the passive layer, more important for the HNO_3-passivated layer than for the air-passivated layer.

As proposed by several authors [4, 23] the examination of the ratio $C^M[Cr2p_{3/2}, oxide]/(C^M[Fe2p_{3/2},$

TABLE IV Passive layers thickness for air-passivated and HNO_3-passivated X20Cr13, X30Cr13, X40Cr14 samples. This thickness was estimated by different methods. The standard deviation for each estimation was 0.25 nm. (met) = metallic species, (ini) = initial concentration, (ox) = oxidized species

	Passivation treatment	Attenuation of $C^M[Fe2p_{3/2}$ (met)]	$C^M[O1s] = C^M[O1s(ini)]/2$	$C^M[Cr2p_{3/2}(met)] = C^M[Cr2p_{3/2}(ox)]$	$C^M[Fe2p(met)] = C^M[O1s]$	Mean value of columns 4, 5, 6 (st. dev.)
X20Cr13	None	6.9 nm	3.6 nm	4.3 nm	3.5 nm	3.8 nm (0.3 nm)
	HNO_3	5.0 nm	2.9 nm	3.3 nm	2.6 nm	2.9 nm (0.2 nm)
X30Cr13	None	5.6 nm	3.6 nm	3.6 nm	3.8 nm	3.7 nm (0.2 nm)
	HNO_3	4.9 nm	2.4 nm	2.7 nm	2.4 nm	2.5 nm (0.2 nm)
X40Cr14	None	8.1 nm	3.8 nm	3.8 nm	3.5 nm	3.7 nm (0.2 nm)
	HNO_3	4.3 nm	2.5 nm	2.5 nm	2.3 nm	2.4 nm (0.2 nm)

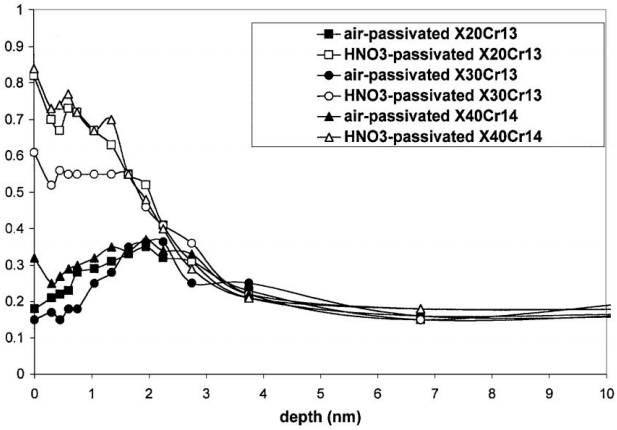

Figure 5 Variation of the ratio $C^M[Cr2p_{3/2}]/C^M[Fe2p_{3/2}]$ as a function of the depth.

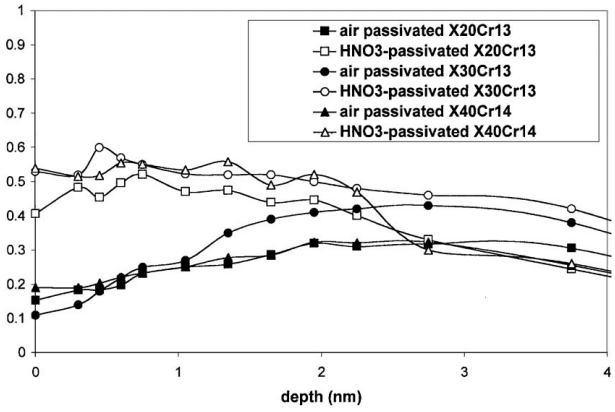

Figure 6 Variation of the protectiveness index Ip with depth. Ip = $C^M[Cr2p_{3/2}$, oxide]/($C^M[Fe2p_{3/2}$, oxide] + $C^M[Cr2p_{3/2}$, oxide]).

oxide] + $C^M[Cr2p_{3/2}$, oxide]) is also pertinent (Fig. 6). This ratio is sometimes called the protectiveness index [4]. A air-passivated sample had a outermost passive layer mainly composed of oxidised iron, up to 80%, the inner layer next to the matrix contains more oxidised chromium up to 40%. A HNO_3-passivated sample had a outermost passive layer mainly composed of oxidised chromium, up to 60%. This amount decreased when we went up to the matrix. The high chromium content in HNO_3-passivated sample layer has been verified on numerous stainless steel [6].

The thickness of the passive layer was estimated by means evolution of the XPS signals. It could be evaluated with attenuation of metallic Fe 2p peak. The metallic Fe 2p peaks was always present, even at the beginning of sputtering. The comparison between intensities at the beginning of sputtering and in the matrix able the evaluation of the attenuating layer thickness. The boundary of this attenuating layer is marked by the stability of all signals. This layer is composed of contamination layer and passive layer. O1s is maximum and C1s is minimum at the end of the contamination layer [24]. The contamination layer is 0.3 nm thick in our case.

Some authors [2, 3, 5] evaluate the passivation layer thickness either—where C^M[O1s] is equal to 50% of its initial value or—where the metallic chromium concentration $C^M[Cr2p_{3/2}$, metal] is equal to the oxidised chromium concentration $C^M[Cr2p_{3/2}$, oxide] or—where the oxygen concentration C^M[O1s] is equal to the metallic concentration of iron $C^M[Fe2p_{3/2}$, metal]. All these evaluations are compared in Table IV. They were close, within 10% except those determined by Fe metal attenuation, which were higher. Indeed, in this latest case, Fe metal signal was the same at this layer boundary than in the matrix. The layers determined by the other methods corresponded to layers where after the layer boundary oxygen, oxidised Cr, oxidised Fe signals still evolved.

The air-formed passive layers were thicker than the HNO_3-passive layers. The same results have been already reported in the literature on other steels [6]. It was suggested that the HNO_3 treatment led to a Cr enrichment of passive layer [10] or removal of inclusions, in particular sulphide inclusions [25]. In our case, samples presented only chromium carbide precipitates. As previously presented [11] HNO_3-passivation did not dissolve the carbide inclusions and led to a Cr enrichment of the passive layer. The amount of carbon in the martensitic steel had no evident influence on the thickness of the passive layer.

To better compare air-passivated and HNO_3-passivated layers, we tentatively modelled these two layers for a X20Cr13 sample. The true concentrations C^T[Cr, oxide], C^T[Fe, oxide], C^T[Fe, metal], C^T[Cr, metal], C^T[O] and C^T[C] were calculated and then integrated over 1 nm thick layers from the surface (O nm) to the matrix (5 nm). These results are presented Figs 7 and 8. These concentrations were also integrated over the whole passive layer in Table V. This table clearly highlighted that air-passivated layer contained less oxidised Cr, less hydroxide and more oxidised Fe than HNO_3-passivated layer. Cr and Fe repartition inside passive layer were different for air-passivated layer and HNO_3-passivated layer. The air-passive layer was

TABLE V Passive layers composition for air-passivated and HNO_3-passivated X20Cr13 sample. The elements atomic concentration were integrated over the passive layer. We arbitrary fixed the total atomic concentration to 100 for a 1 nm thick layer

Passivation treatment	Thickness	[Fe, met]	[Fe, ox]	[Cr, met]	[Cr, ox]	[O^{2-}]	[OH^-]	[C]	Total
None	4 nm	10	90	0	30	170	40	60	400
HNO_3	3 nm	0	40	0	50	120	50	40	300

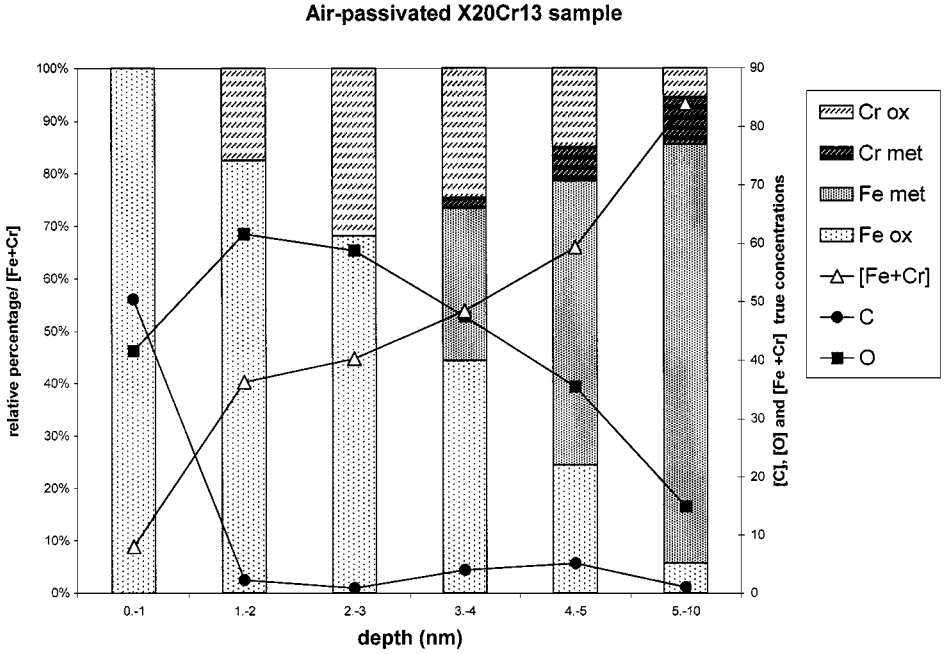

Figure 7 Passive layer model for X20Cr13 air-passivated sample. Integrated C^{T}(O1s] and C^{T}[C1s] and C^{T}[Cr + Fe] were presented (Y axis on the right). For each depth interval, integrated C^{T}[O1s] + C^{T}[C1s] + C^{T}[Cr + Fe] = 100. Integrated C^{T}[Cr2$p_{3/2}$, oxide], C^{T}[Fe2$p_{3/2}$, oxide], C^{T}[Cr2$p_{3/2}$, metal] and C^{T}[Fe2$p_{3/2}$, metal] were ratioed by C^{T}[Cr + Fe]. The calculated percentage were presented (Y axis on the left). C^{T}[Cr + Fe] = C^{T}[Cr2$p_{3/2}$, oxide] + C^{T}[Fe2$p_{3/2}$, oxide] + C^{T}[Cr2$p_{3/2}$, metal] + C^{T}[Fe2$p_{3/2}$, metal].

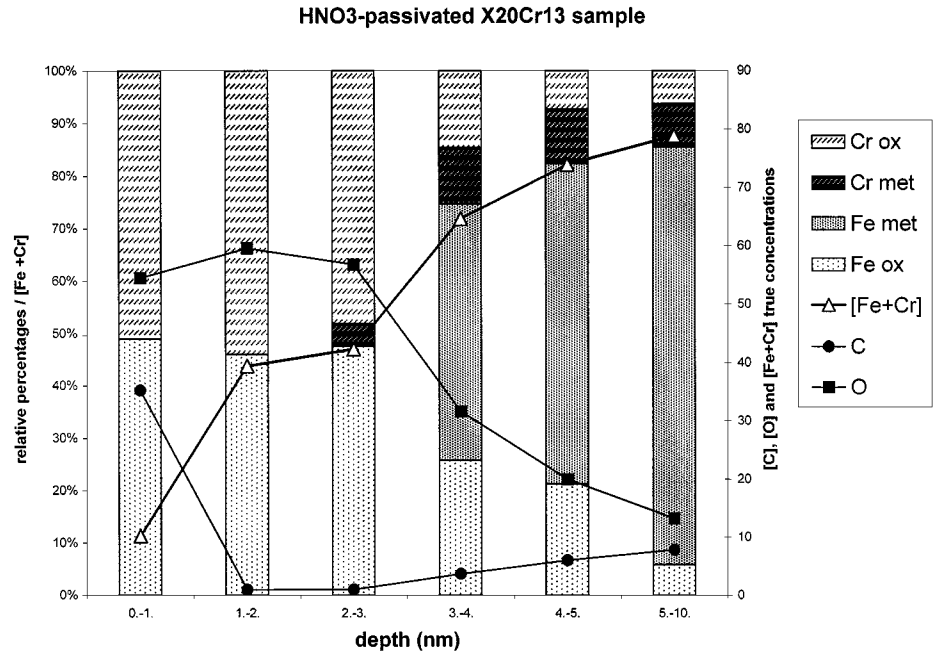

Figure 8 Passive layer model for X20Cr13 HNO_3-passivated sample. Integrated C^{T}[O1s] and C^{T}[C1s] and C^{T}[Cr + Fe] were presented (Y axis on the right). For each depth interval, integrated C^{T}[O1s] + C^{T}[C1s] + C^{T}[Cr + Fe] = 100. Integrated C^{T}[Cr2$p_{3/2}$, oxide], C^{T}[Fe2$p_{3/2}$, oxide], C^{T}[Cr2$p_{3/2}$, metal] and C^{T}[Fe2$p_{3/2}$, metal] were ratioed by C^{T}[Cr + Fe]. The calculated percentage were presented (Y axis on the left). C^{T}[Cr + Fe] = C^{T}[Cr2$p_{3/2}$, oxide] + C^{T}[Fe2$p_{3/2}$, oxide] + C^{T}[Cr2$p_{3/2}$, metal] + C^{T}[Fe2$p_{3/2}$, metal].

mainly constituted of oxidised iron at the surface. Oxidised chromium seems to be localised at the interface with the matrix. HNO_3-passive layer contained the same proportion of oxidised Cr and oxidised Fe. Separation between oxidised elements and metallic elements was clearer in HNO_3-passive layer than in air-passive layer.

4. Conclusion

The present study using XPS and electrochemical measurements on three martensitic stainless steels used for surgical instrumentation leads to the following conclusions:

HNO_3-passivation treatment was efficient to enhance the pitting resistance of the steel. The formed layer was thinner than the one observed on air-formed film. This HNO_3-formed layer was enriched in oxidised chromium and hydroxide. Oxidised chromium and iron seem to be uniformly distributed all over the passive layer. In air-passivated layer, oxidised iron is concentrated at the surface and oxidised chromium is localised at the interface passive layer-matrix.

The amount of carbon in the martensitic steel had no evident influence on the corrosion resistance and on the composition and thickness of the passive layer.

References

1. I. REYNAUD, M. VAYER, J. P. KAUFFMANN and R. ERRE, in Eurocorr'96 Proceeding (1996) Vol. 8, p. 6.
2. P. BRUESCH, K. MÜLLER, A. ATRENS and H. NEFF, *Appl. Phys A* **38** (1985) 1.
3. J. GLUSZEK, G. B. FREEMAN, J. BARON and J. KUBICKI, *Corrosion Nace* **41** (1985) 527.
4. W. P. YANG, D. COSTA and P. MARCUS, *J. Electrochem. Soc.* **141** (1994) 2669.
5. S. JIN and A. ATRENS, *Appl. Phys. A* **42** (1987) 149.
6. K. ASAMI and K. HASHIMOTO, *Corrosion Science* **19** (1979) 1007.
7. T. HONG, T. OGUSHI and M. NAGUMO, *ibid.* **38** (1996) 8881.
8. C. HUBSCHMID, D. LANDOLT and H. J. MATHIEU, *Fresenius J. Anal. Chem* **353** (1995) 234.
9. T. SHIBATA and T. TAKEYAMA, in Proceedings of the 19th Symposium on Corrosion and Protection (Japan Society of Corrosion Engineering, 1978) p. 23.
10. T. HONG and M. NAGUMO, *Corrosion Science* **39** (1997) 1665.
11. I. REYNAUD-LAPORTE, M. VAYER, J. P. KAUFFMANN and R. ERRE, *Microsc. Microanal. Microstruct.* **8** (1997) 175.
12. R. QVARFORT, *Corrosion Science* **28** (1988) 135.
13. H. J. MATHIEU and D. LANDOLT, *Appl. of Surf. Sci.* **3** (1979) 348.
14. R. L. TAPPING, R. D. DAVISION and T. E. JACKMANN, *Surface and Interface Analysis* **7** (1995) 105.
15. M. P. SEAH and W. A. DENCH, *Surf. Interf. Anal.* **1** (1979) 2.
16. C. R. CLAYTON and Y. C. LU, *J. Electrochem.* (1986) 2465.
17. R. DEVAUX, D. VOUAGNER, A. M. DE BECDELIEVRE and C. DURET-THUAL, *Corros. Sci.* **36** (1994) 171.
18. T. E. POU and J. O. M. BOCKRIS, *J. of Electrochem. Soc.* **131** (1984) 1243.
19. R. NOVAK, P. HESS, H. OETZMANN and C. SCHIMDT, *Applied Surface Science* **43** (1989) 11.
20. G. P. HALADA and C. R. CLAYTON, *J. Vac. Sci. Technol.* **11** (1993) 2342.
21. R. LECLERCQ, M. KAMAL, J. F. LAMONIER and L. LECLERCQ, *Applied Catalysis A* **121** (1995) 169.
22. M. NAKAZAWA and H. OKAMOTO, *Appl. Surf. Sci.* **24** (1985) 75.
23. R. KIRCHHEIM, B. HEINE, H. FISHMEISTER, S. HOFMANN, H. KNOTE and U. STOLZ, *Corrosion Science* **29** (1989) 899.
24. J. R. CAHOON and R. BANDY, *Corrosion Nace* **38** (1982) 299.
25. M. A. BARBOSA, A. GARRIDO, A. CAMPILHO and I. SUTHERLAND, *Corrosion Sci.* **32** (1991) 179.

Received 30 July 1998
and accepted 23 November 1999